

Deletion of the auxiliary $\alpha_2\delta_1$ voltage sensitive calcium channel subunit in osteocytes and late-stage osteoblasts impairs femur strength and load-induced bone formation in male mice

Christian S. Wright^{1,2}, Karl J. Lewis³, Katelyn Semon^{1,4}, Xin Yi^{1,2}, Perla C. Reyes Fernandez^{1,2}, Katie Rust¹, Matthew Prideaux², Artur Schneider⁵, Molly Pederson⁶, Padmini Deosthale⁴, Lilian I. Plotkin^{2,4} , Julia M. Hum⁵, Uma Sankar^{2,4}, Mary C. Farach-Carson⁷, Alexander G. Robling^{2,4}, William R. Thompson^{1,2,4,*}

¹Department of Physical Therapy, School of Health and Rehabilitation Sciences, Indiana University, Indianapolis, IN 46202, United States

²Indiana Center for Musculoskeletal Health, Indianapolis, IN 46202, United States

³Department of Biomedical Engineering, Cornell University, Ithaca, NY 14850, United States

⁴Department of Anatomy & Cell Biology, School of Medicine, Indiana University, Indianapolis, IN 46202, United States

⁵Department of Physiology, College of Osteopathic Medicine, Marian University, Indianapolis, IN 46202, United States

⁶School of Science, Indiana University-Purdue University, Indianapolis, IN 46202, United States

⁷Department of Diagnostic and Biomedical Sciences, School of Dentistry, University of Texas, Health Science Center, Houston, TX 78712, United States

*Corresponding author: William R. Thompson, Department of Physical Therapy, School of Health and Rehabilitation Sciences, Indiana University, Indianapolis, IN 46202, United States (thompwil@iu.edu).

Abstract

Osteocytes sense and respond to mechanical force by controlling the activity of other bone cells. However, the mechanisms by which osteocytes sense mechanical input and transmit biological signals remain unclear. Voltage-sensitive calcium channels (VSCCs) regulate calcium (Ca^{2+}) influx in response to external stimuli. Inhibition or deletion of VSCCs impairs osteogenesis and skeletal responses to mechanical loading. VSCC activity is influenced by its auxiliary subunits, which bind the channel's α_1 pore-forming subunit to alter intracellular Ca^{2+} concentrations. The $\alpha_2\delta_1$ auxiliary subunit associates with the pore-forming subunit via a glycosylphosphatidylinositol anchor and regulates the channel's calcium-gating kinetics. Knockdown of $\alpha_2\delta_1$ in osteocytes impairs responses to membrane stretch, and global deletion of $\alpha_2\delta_1$ in mice results in osteopenia and impaired skeletal responses to loading in vivo. Therefore, we hypothesized that the $\alpha_2\delta_1$ subunit functions as a mechanotransducer, and its deletion in osteocytes would impair skeletal development and load-induced bone formation. Mice (C57BL/6) with LoxP sequences flanking *Cacna2d1*, the gene encoding $\alpha_2\delta_1$, were crossed with mice expressing Cre under the control of the Dmp1 promoter (10 kb). Deletion of $\alpha_2\delta_1$ in osteocytes and late-stage osteoblasts decreased femoral bone quantity ($P < .05$) by DXA, reduced relative osteoid surface ($P < .05$), and altered osteoblast and osteocyte regulatory gene expression ($P < .01$). *Cacna2d1^{fl/fl}*, Cre + male mice displayed decreased femoral strength and lower 10-wk cancellous bone in vivo micro-computed tomography measurements at the proximal tibia ($P < .01$) compared to controls, whereas *Cacna2d1^{fl/fl}*, Cre + female mice showed impaired 20-wk cancellous and cortical bone ex vivo micro-computed tomography measurements ($P < .05$) vs controls. Deletion of $\alpha_2\delta_1$ in osteocytes and late-stage osteoblasts suppressed load-induced calcium signaling in vivo and decreased anabolic responses to mechanical loading in male mice, demonstrating decreased mechanosensitivity. Collectively, the $\alpha_2\delta_1$ auxiliary subunit is essential for the regulation of osteoid-formation, femur strength, and load-induced bone formation in male mice.

Keywords: osteocytes, $\alpha_2\delta_1$ subunit, voltage-sensitive calcium channel, mechanotransduction, load-induced bone formation

Lay Summary

The ability of bone to sense and respond to forces generated during daily physical activities is essential to skeletal health. Although several bone cell types contribute to the maintenance of bone health, osteocytes are thought to be the primary mechanosensitive cells; however, the mechanisms through which these cells perceive mechanical stimuli remains unclear. Previous work has shown that voltage sensitive calcium channels are necessary for bone to sense mechanical force; yet the means by which those channels translate the physical signal into a biochemical signal is unclear. Data within this manuscript demonstrate that the extracellular $\alpha_2\delta_1$ subunit of voltage sensitive calcium channels is necessary for load-induced bone formation as well as to enable calcium influx within osteocytes. As this subunit enables physical interactions of the channel pore with the extracellular matrix, our data demonstrate the need for the $\alpha_2\delta_1$ subunit for mechanically induced bone adaptation, thus serving as a physical conduit through which mechanical signals from the bone matrix are transduced into biochemical signals by enabling calcium influx into osteocytes.

Introduction

Skeletal unloading due to disability, aging, or disease dramatically increases bone resorption and suppresses bone formation,¹ leading to bone loss,² increased fracture risk, and impaired quality of life.³ These physical impairments constitute a significant financial burden to the U.S. economy, with \$5.7 billion in Medicare cost alone in 2016.⁴⁻⁶ Conversely, mechanical loading is anabolic for bone,⁷ resulting in increased bone formation, BMD, and improved skeletal morphology.^{8,9} As such, understanding the mechanisms underlying skeletal responses to mechanical loading can generate effective therapeutic interventions to curtail the financial burden and quality of life impairments associated with osteoporosis.¹⁰

Osteocytes are the most abundant and mechanosensitive cells within the skeleton, comprising 90%–95% of the total bone cell population.¹¹ Although it is well-established that these terminally differentiated, stellate cells sense and respond to mechanical force, influencing both bone formation and resorption via osteoblast and osteoclast activity,¹² it remains unclear how mechanical forces are transmitted through cell surface receptors to initiate intracellular anabolic responses.

The first measurable response of bone cells to mechanical stimuli is a rapid and transient increase in intracellular calcium (Ca^{2+}).^{13,14} As such, voltage-sensitive calcium channels (VSCCs) play a pivotal role in skeletal development and bone formation.¹⁵ Several *in vivo* studies support the fundamental function of VSCCs on bone homeostasis, as VSCC inhibition impairs skeletal development^{16,17} and inhibits osteogenesis,¹⁸ resulting in vertebral defects, decreased mechanosensitivity,¹⁹ and impaired bone formation.^{17,20,21} As osteocytes are highly sensitive to mechanical loading, they represent a prime cell type through which VSCCs may influence bone formation and skeletal development.

VSCCs form a multi-protein complex composed of a pore-forming α_1 subunit and several auxiliary subunits, including $\alpha_2\delta_1$, β , and γ (Figure 1). The pore-forming α_1 subunit facilitates Ca^{2+} entry, while the auxiliary subunits associate with the channel pore and regulate channel activity.^{15,22} Positioned entirely extracellular via a glycosylphosphatidylinositol (GPI) anchor, the $\alpha_2\delta_1$ auxiliary subunit associates with the pore-forming subunit to regulate the channel's Ca^{2+} gating kinetics, membrane density, and interactions with the extracellular matrix and/or ligands.²²⁻²⁴ Although numerous studies have shown that VSCCs contribute to skeletal mechanosensitivity,^{17,19-21} the function of VSCCs within osteocyte mechanotransduction remains unclear. We recently found that the $\alpha_2\delta_1$ auxiliary subunit binds tightly to the large heparan sulfate proteoglycan perlecan (PLN).²⁵ This physical connection creates a mechanical tether that spans the lacunocanalicular space,²⁶ directly connecting the VSCC gating apparatus $\alpha_2\delta_1$ to mineralized bone and thereby providing a physical means to transmit mechanical forces to the osteocyte cell membrane.²⁷ Although our studies in cultured osteocytes showed decreased mechanical responses following $\alpha_2\delta_1$ knockdown,²⁸ the function of $\alpha_2\delta_1$ in osteocytes *in vivo* has yet to be established.

The objective of this study was to determine the cell-specific function of $\alpha_2\delta_1$ on skeletal development and load-induced bone formation via conditional deletion of $\alpha_2\delta_1$ in osteocytes. We hypothesized that deletion of $\alpha_2\delta_1$ late in the osteogenic lineage would impair skeletal development, bone formation, and mechanosensitivity *in vivo*.

Materials and Methods

Mice

Osteocyte-targeted deletion of *Cacna2d1*, the gene encoding $\alpha_2\delta_1$, was achieved using the Cre-LoxP (locus of x-over, P1) system as previously described.²⁹ Briefly, the targeted mice harboring LoxP sequences (34 bp) flanking crucial exons of *Cacna2d1* were developed as described³⁰ and crossed with mice expressing Cre under the control of the mouse dentin matrix protein-1 (*Dmp1*) promoter (10 kb).³¹ For longitudinal experiments, *Cacna2d1^{fl/fl}*, Cre+ males were bred with *Cacna2d1^{fl/fl}*, Cre- females to produce Cre+ and Cre- pups, each of which were homozygous for the floxed allele (denoted as *Cacna2d1^{fl/fl}*). For all experiments, *Cacna2d1^{fl/fl}*, Cre- littermates were used as controls. From this point forward, *Cacna2d1^{fl/fl}*, Cre- mice will be referred to as “Cre-” and *Cacna2d1^{fl/fl}*, Cre+ mice as “Cre+.” Cre-mediated recombination of floxed alleles was confirmed by quantifying *Cacna2d1* expression via real-time PCR of purified osteocyte-enriched cultures extracted from cortical bone tissue. Mice were genotyped for the presence of LoxP sites within the *Cacna2d1* gene and the *Dmp1*-Cre transgene by PCR using DNA isolated from tail tips. For *Cacna2d1*-floxed alleles, the forward primer, 5'-GGGCTCTTCTTCTTTAGTAC-3', and the reverse primer, 5'-AATCTCAGGATTTACTACTAC-3', were used to generate a PCR product of 227 bp. The forward primer was located proximal to exon 6 (the floxed region), and the reverse primer was located distal to the 3' LoxP site. As an internal control, exon 6 (unmodified) was also amplified by PCR. Primers for the 9.6kb *Dmp1*-Cre transgene were used as previously published.³¹ Both male and female littermate mice used in all experiments were housed under a 12-h light-dark cycle (7 AM-7 PM; group housed by sex and litter) and were given standard mouse chow (2018SX, Harlan-Teklad; 1% Ca; 0.65% P; 2.1 IU/g vitamin D₃) and water ad libitum. Experimental mice were housed 5 mice per cage, while breeders were housed 1:1, according to the policies of Indiana University animal facilities. Investigators were blinded to genotype during all experimental procedures.

For *in vivo* imaging experiments of load-induced Ca^{2+} signaling, expression of the fluorescent Ca^{2+} sensor GCaMP6f³² was achieved by crossing Ai95 mice (bearing the GCaMP6f gene behind a Lox-STOP-Lox codon³²; Jackson Labs) with *Dmp1*-Cre mice (9.6 kb).³¹ As expression of GCaMP6f and conditional deletion of *Cacna2d1* are both regulated by the presence of Cre, the experimental groups consisted of mice (1) positive for GCaMP6f, *Cacna2d1^{+/+}*, *Dmp1* Cre+ and (2) positive for GCaMP6f, *Cacna2d1^{fl/fl}*, *Dmp1* Cre+. Thus, the presence of Cre induced expression of GCaMP6f in both conditions; however, in control mice (denoted as “G^{+/+}”), the *Cacna2d1* gene was not floxed, while both alleles of the *Cacna2d1* gene of conditional KO mice were floxed (denoted as “G^{fl/fl}”). Thus, in G^{+/+} mice, Cre will activate the expression of GCaMP6f, but will not delete *Cacna2d1*, whereas in G^{fl/fl} mice, Cre will both activate GCaMP6f and induce recombination of floxed *Cacna2d1* alleles with subsequent loss of expression in osteocytes. A sample size of 8 per sex and genotype (G^{+/+} and G^{fl/fl}) was tested, as previous reports showed it to be the minimum number of mice required to derive differences.³³ All mice were on the C57BL/6 background. All procedures were approved by Indiana University's IACUC.

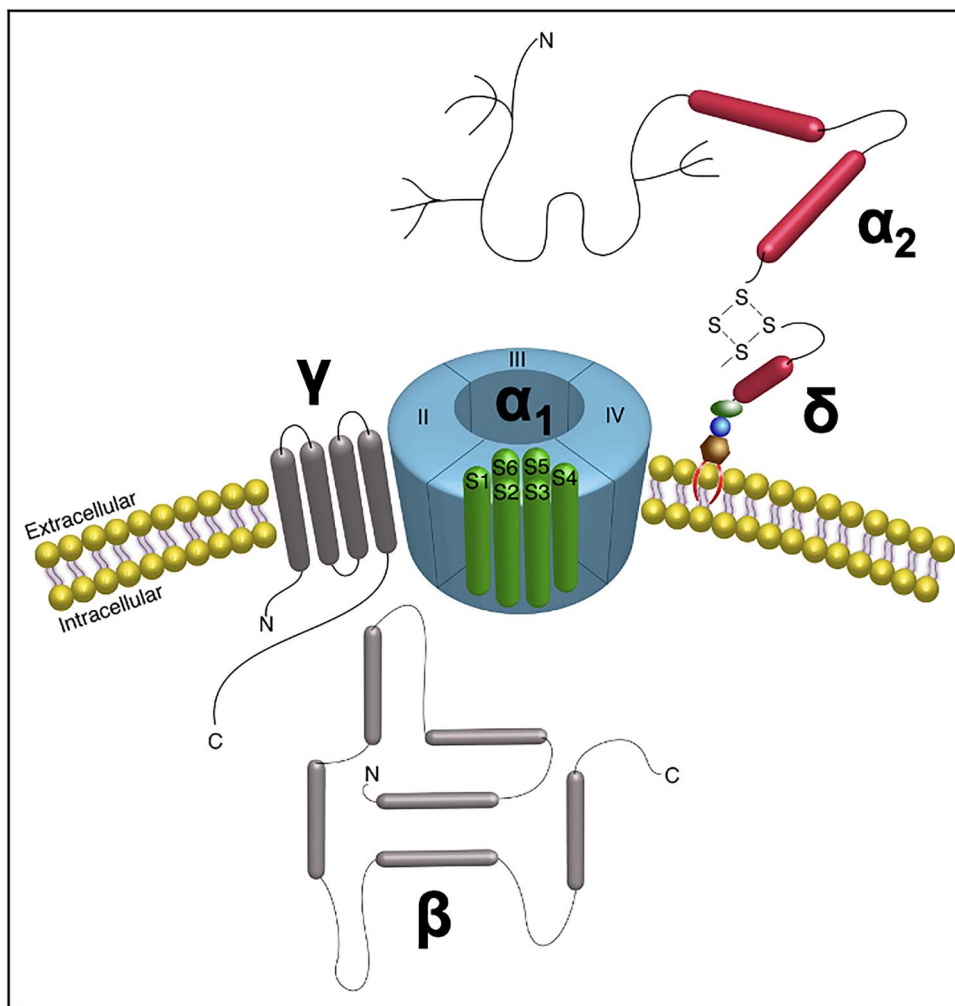


Figure 1. Voltage-sensitive calcium channel (VSCC) structure. The VSCC complex is composed of the α_1 pore-forming subunit and the auxiliary subunits β , γ , and $\alpha_2\delta$, which associate with the channel to alter its gating kinetics. The extracellular $\alpha_2\delta$ subunit is anchored to the membrane via a GPI anchor. Illustration from previously published image (Wright CS, Curr Osteoporos Rep 2021).

To verify that the $\alpha_2\delta_1$ auxiliary subunit is the predominant isoform expressed in osteocytes, IDG-SW3 cells, a commonly used osteocyte cell line,³⁴ were differentiated in osteogenic media for 15 d, and mRNA levels of each subunit isoform were quantified.

Dual-energy X-Ray Absorptiometry

Longitudinal DXA measurements were collected on live mice every 3 weeks from 6 to 16 wk of age using an UltraFocus digital X-ray cabinet (Hologic Faxitron®) as previously described.³⁵ Briefly, mice were anesthetized with isoflurane (2.5%, IsoFlo, Abbott Laboratories) mixed with oxygen (O_2 , 1.5 L/min) for ~8 min, including induction and scanning. Mice were placed on the scanner in a prone position, while whole body scans were analyzed regionally using the Lunar region of interest (ROI) tools. The ROI for the spine included from the second (L2) through fifth (L5) lumbar vertebrae. The ROI for the right femur included bone between the acetabulum and the tibiofemoral joint space. The ROI for the whole body included all skeletal tissues caudal to the boundary between the skull and the first cervical vertebra but excluded the tail. BMC was measured, and BMD was derived for each ROI scan.

In Vivo Micro-Computed Tomography

At 10 wk of age, left proximal tibias were scanned using micro-computed tomography (μ CT) (Skyscan 1176, Bruker-microCT, Kontich, Belgium) and host software (1176 version 1.1, Bruker-microCT). Mice were anesthetized with isoflurane dissolved in oxygen (2.5%, IsoFlo, Abbott Laboratories) before transitioning to the scanning bed and a nose cone to maintain anesthesia (0.5%–5% delivery rate) throughout the scanning process (~15 min). Each mouse was positioned on its back with its left leg extended on top of a piece of foam and secured in place with masking tape. Scans were taken at a 9 μ m resolution, with scanning parameters consisting of 50 kV, 500 μ A, and 0.9° rotation step.

Ex Vivo μ CT

Tibiae and femora were dissected at 20 wk of age and fixed in NBF (10%, v/v) for at least 48 h and then placed in ethanol (EtOH, 70%, v/v) for evaluation. Bones were scanned, reconstructed, and analyzed as previously described.³⁵ Briefly, scans were collected using a Scanco μ CT-35 tomographer (Scanco Medical) at 10 μ m resolution, 50-kV peak tube potential, and 151-ms integration time. The distal 60% and mid-shaft 50% of the femur, and the proximal 40% and mid-shaft 50% of the

tibia were scanned. Standard parameters related to cancellous and cortical bone architecture were measured.³⁶ To quantify morphological changes following tibial axial compression, μ CT-derived cortical bone responses of the loaded tibia were normalized to the contralateral unloaded tibia to derive a delta change value (Load—Unloaded Tibia).

In Vivo Tibial Axial Loading

To induce anabolic skeletal responses, tibial axial compression was applied to *Cacna2d1^{fl/fl}* Cre+ and *Cacna2d1^{fl/fl}*, Cre– mice as previously described.⁵ Briefly, 6 mice of each sex and genotype ($N=24$) were euthanized at 16 wk of age to be used for calibration strain measurements. The right hindlimb was disarticulated and frozen (-20°C) until strain gauge testing. A single-element strain gauge (EA-06-015DJ-120; Vishay Precision Group) was applied to the posterior surface of the tibial midshaft (between the tibia and fibula), and the microstrain:load ratio was measured for each sample using progressively increasing load applications, while simultaneously recording the voltage output from the load cell and strain gauge. All tests were averaged within each genotype and sex to determine the microstrain:load ratio. A peak value of 3000 $\mu\epsilon$ was chosen and applied to all genotypes. This peak $\mu\epsilon$ corresponded to peak loads of 8.71 N (male, Cre –), 8.21 N (male, Cre +), 7.80 N (female, Cre –), and 7.61 N (female, Cre +). At 18 wk of age, mice of each sex and Cre status ($n=11-15$) began the tibial axial compression protocol. Mice were anesthetized using isoflurane inhalation, and their right hindlimb (knee to calcaneus) was loaded using sinusoidal (haversine) waveform (2 Hz, 180 cycles, no intercycle rest period) to the peak load determined by strain gauging (see above). Five loading bouts were applied over a 10-d period with a day of rest between each bout. S.C. injection of calcein (10 mg/kg) was administered 1 d before the final loading bout, followed by a S.C. injection of alizarin (20 mg/kg) 10 d later. Mice were euthanized 13 d after the final bout of loading (20 wk of age). Both tibiae were harvested and placed in NBF (10%, v/v) for 48 h then stored in EtOH (70%, v/v) at 4°C until histological analysis.

In Vivo Mechanical Loading and Calcium Responses

Osteocyte Ca^{2+} signaling in response to mechanical loading in vivo was examined in the mid-diaphysis of the right third metatarsal (MT3) of $\text{G}^{+/+}$ and $\text{G}^{fl/fl}$ mice as recently reported^{33,37} and depicted in Figure 2. Load–strain–displacement relationships for both $\text{G}^{+/+}$ and $\text{G}^{fl/fl}$ mice were generated using methods previously reported (data not shown).³³ MT3 bones were loaded in a 3-point bending device at 1 Hz to mid-diaphyseal strain levels of 250, 500, 1000, 2000, and 3000 $\mu\epsilon$. These levels encompass the range of strains that have been reported during physiological activities from in vivo strain gauge studies, with strains up to 2000 $\mu\epsilon$ characteristic of habitual activities, while strains on the order of 3000 $\mu\epsilon$ are seen in more extreme loading activities.^{31,32} All loading procedures were carried out under anesthesia with isoflurane. First, the dorsal surface of the MT3 was accessed by a single scalpel incision through the skin and extensor aponeurosis, with care taken to isolate and avoid the dorsal foot arteries. The lower stainless-steel 1 mm diameter cylinder fulcrum pin of the 3-point bending device was inserted beneath the mid-diaphysis of the MT3, thus

functionally isolating the bone. The pin was placed in its anchor bracket and the entire foot positioned in the PBS bath (37°C) of the loading apparatus. The upper stainless steel loading contacts then were positioned on the dorsal bone surface, and a nominal tare strain ($\sim 100 \mu\epsilon$) was applied to prevent the bone from moving during loading. The entire apparatus was set onto the stage of a multiphoton microscope (MPM; Thor Labs) equipped with a tunable Ti-sapphire laser light source for in vivo osteocyte imaging studies (Coherent). Bones were loaded cyclically under displacement control to achieve the desired strain level using a haversine waveform at 1 Hz using a custom loading device; coefficients of variation for each target strain level were previously determined to be $\sim 15\%$. The duration of each strain-loading bout was 60 s and was performed with simultaneous osteocyte imaging using the MPM. The loading bout was followed by 15 min of rest. The loading and rest procedure was then repeated for the next test strain level until the complete test strain range (250–3000 $\mu\epsilon$) was covered.

Image Acquisition and Analysis

Multiphoton imaging was performed at the dorsal mid-shaft region of the MT3 in vivo, with osteocytes sampled in a plane located $\sim 20 \mu\text{m}$ below the periosteal surface. Osteocyte Ca^{2+} imaging was performed using a water immersion objective (20x, Olympus LUMPLFLN) focused on the mid-diaphysis. Excitation was at 920 nm wavelength, and a 490–560 nm bandpass filter was used for detection. Time series images were acquired at a rate of 10 frames per second. Ca^{2+} intensity measurements were performed by post-processing time series images using ImageJ (NIH). Individual osteocytes were delineated, and mean pixel intensity values were collected in each frame before and during loading. The intensities for each cell of interest were normalized to the mean baseline intensity for that cell over a 30-s period prior to the start of cyclic loading. Responding osteocytes were defined as those cells showing a $> 25\%$ increase in normalized fluorescence intensity during loading. Figure 2 shows an example of the fluorescence intensity changes typically seen in cells that respond to mechanical loading. In addition to counting the number of cells, the fold increase in mean intensity during loading compared to non-loaded baseline was also analyzed.

Mechanical Testing

Parameters related to whole bone strength were measured using 3-point bending tests on isolated femora as previously described.³⁸ Briefly, each femur was loaded to failure in monotonic compression, during which force and displacement measures were collected every 0.01 s. Ultimate force, energy to ultimate failure, and stiffness were calculated from the force/displacement curves, using standard equations.³⁹

RNA Isolation and Real-Time PCR

Total RNA was isolated from whole ulnas of Cre– and Cre+ mice. Ulnas were dissected with all soft tissue removed, including the periosteum, and immediately flash-frozen in liquid N_2 . To isolate RNA, ulnas were homogenized in TRIzol using the Bullet Blender[®] Tissue Homogenizer (Next Advance) and the soluble fraction was removed. Total RNA was isolated through phenol-chloroform extraction and subsequent RNeasy Plus kit (Qiagen) as described.⁴⁰ mRNA

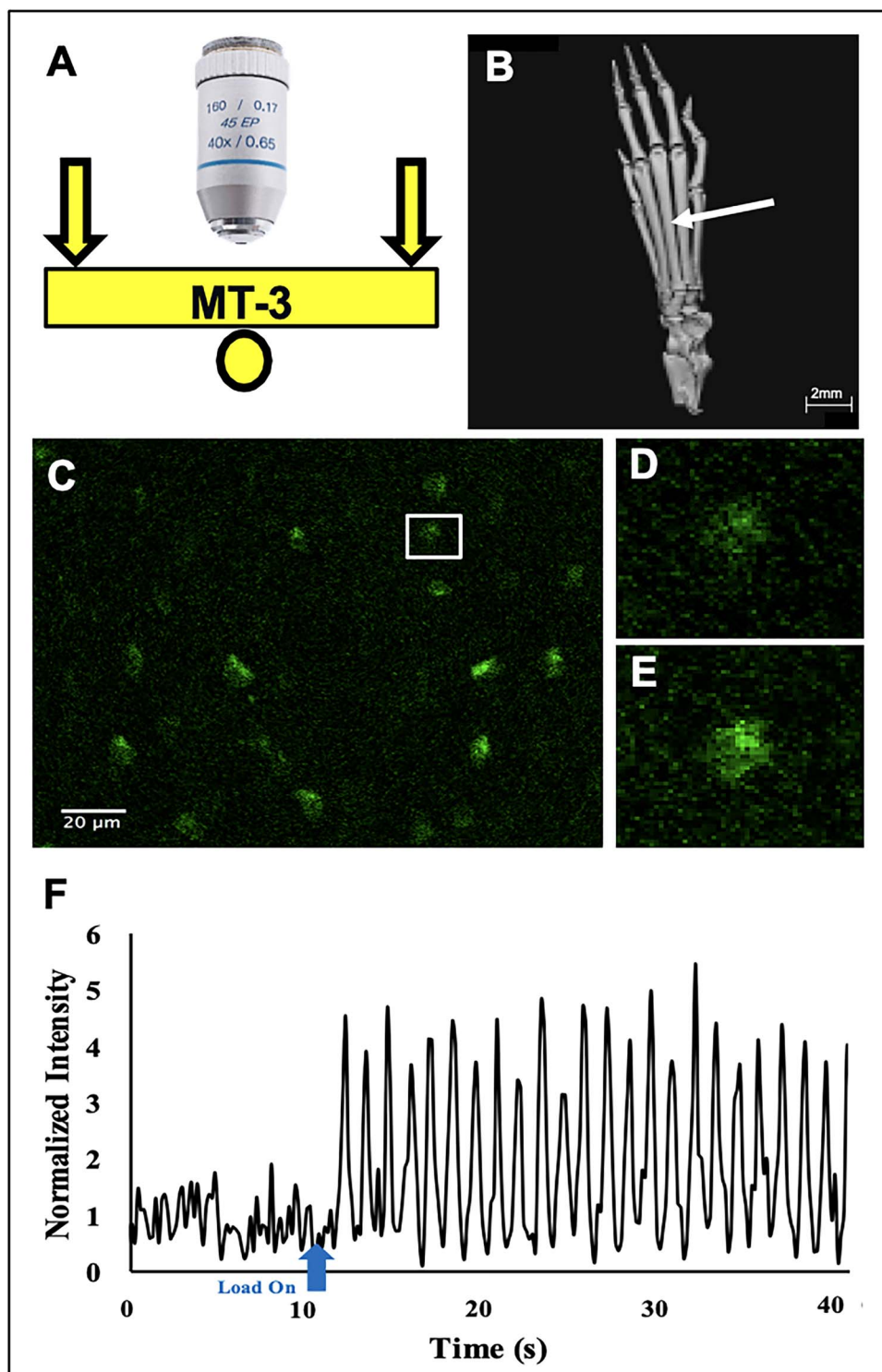


Figure 2. In vivo MT3 mechanical loading and calcium responses. (A) Schematic of microscope objective and loading configuration for the MT3 bone. (B) μ CT scan of mouse hind paw showing MT3 (arrow). (C) Representative image of OtGP3 osteocytes fluorescing at baseline with one cell blown up to show the difference between (D) baseline fluorescence vs (E) increases seen during mechanical loading. (F) Representative trace of a single osteocyte Ca^{2+} signaling fluorescence intensity both before and during loading.

was reverse transcribed, and genes were amplified with a BioRad CFX Connect qPCR machine, using osteogenic- and osteoclast-specific gene primers (Supplementary Table S1). PCR products were normalized to *GAPDH* or *GUSB* and quantified using the $\Delta\Delta\text{CT}$ method (denoted in figures as $2^{\Delta\Delta\text{Cq}}$).

Histological Processing

Femora and tibiae were dehydrated in graded alcohols, cleared in xylene, and embedded in methylmethacrylate following standard protocols.⁴¹ For static histomorphometry measurements, distal left femur sections were cut approximately 5 μ m in thickness in the coronal plane, using a motorized microtome

(Leica Microsystems, Inc.) equipped with a tungsten carbide knife. To measure load-induced bone formation, thick-cut sections were taken from the tibia midshaft, approximately 3 mm distal to the tibiofibular junction, and manually ground down to approximately 30 μm . A single unstained section of the tibial diaphysis from loaded and unloaded bones was imaged digitally on a fluorescent microscope using filter sets that provided excitation and emission for the calcein and alizarin wavelengths, administered at 17 and 19 wk of age, respectively. Digital images were imported into ImagePro Express (Media Cybernetics, Inc.), and the following histomorphometric measurements were recorded for the periosteal surface: total perimeter, single label perimeter (sL.Pm), double label area (dL.Ar) and perimeter (dL.Pm), total bone and marrow area. The following results were calculated: mineral apposition rate ($\text{MAR} = \text{dL.Ar}/\text{dL.Pm}/11 \text{ d}$), mineralizing surface ($\text{MS}/\text{BS} = (0.5 \times \text{sL.Pm} + \text{dL.Pm})/\text{total perimeter} \times 100$), and bone formation rate ($\text{BFR}/\text{BS} = \text{MAR} \times \text{MS}/\text{BS} \times 3.65$). All measurements were collected such that the operator was blinded to genotype. Histology sections, staining, and analyses were conducted by the Histology Core Facilities within the Indiana Center for Musculoskeletal Health.

MMA-embedded, thin sections were deplasticized in acetone and stained by 2 different procedures: (1) a modification of the von Kossa/MacNeal's (VKM) Tetrachrome protocol⁴² and (2) a tartrate acid-resistant acid phosphatase (TRAP) stain.⁴³ For VKM-stained slides, mineralized bone was stained using the Von Kossa silver method, and the unmineralized tissue was counter-stained with MacNeal's tetrachrome. For TRAP staining, sections were pre-incubated in acetate buffer (0.2 M, pH = 5.0), rinsed, and incubated in a warmed acid phosphatase solution. Sections then were counterstained with Toluidine Blue, air-dried, and cover-slipped with an aqueous-based mounting media. Histomorphometric analysis was performed using the OsteoMeasure high-resolution digital video system (OsteoMetrics Inc.) Images were taken using an Olympus BX51 fluorescent microscope and Olympus cellSens Entry 1.2 (Build 7533) imaging software. Standard nomenclature was used according to the Histomorphometry Nomenclature Committee of the American Society of Bone and Mineral Research.⁴⁴

Statistical Analyses

Statistical variance was expressed as the means \pm SEM. Statistical significance was evaluated using repeated measures (RM) of ANOVA, 2-way ANOVA, linear regression analysis, or unpaired Student's *t* test, and post hoc analyses using Šidák's multiple comparisons test as appropriate (Prism GraphPad, Version 9.5.1). Outliers were detected in measurements of bone quantity and bone quality and were excluded according to the outlier labeling rule.⁴⁵ Values were considered significant if $P \leq .05$. qPCR and Western blot assays were replicated at least 3 times to assure reproducibility. The number of animals used is denoted for individual experiments.

Results

Deletion of $\alpha_2\delta_1$ in Dmp1-expressing cells had no effect on body or femur length

To test for *Cacna2d1* expression, the gene encoding $\alpha_2\delta_1$, qPCR was performed using mRNA from primary osteocytes

of Cre⁻ and Cre⁺ mice. *Cacna2d1* mRNA levels were significantly lower in osteocytes from Cre⁺ mice compared to those derived from Cre⁻ controls (Figure 3A). To determine which of the 4 variants of the $\alpha_2\delta_1$ subunit are predominantly expressed in osteocytes, mRNA levels of each subunit were quantified in differentiated IDG-SW3 cells, a commonly used osteocytic cell line.³⁴ Levels of *Cacna2d1* transcripts were higher than *Cacna2d2* (400-fold), *Cacna2d3* (67-fold), and *Cacna2d4* (4 million-fold), demonstrating that $\alpha_2\delta_1$ is the predominant $\alpha_2\delta$ subunit variant in osteocytes (Figure 3B) and further confirming previous findings from our lab.²⁸ Body length (snout to rump) and femur length were measured in Cre⁻ and Cre⁺ mice, and no differences were observed (Figure 3C and D).

Deletion of $\alpha_2\delta_1$ in Dmp1-expressing cells decreased femoral bone quantity

To determine the function of the $\alpha_2\delta_1$ subunit in osteocytes on skeletal formation, longitudinal DXA measurements were taken every 3 weeks from 6 to 16 wk of age in both male and female Cre⁻ and Cre⁺ mice (Figure 4). In male mice, no differences were observed between Cre⁻ and Cre⁺ mice for BMD of the whole body, spine (L2–L5), or femur longitudinally (Figure 4A). Cre⁺ male mice showed reduced femur BMC compared to Cre⁻ mice longitudinally, with single timepoint differences between genotypes for the whole body (12 and 16 wk) and spine BMC (12 wk, Figure 4A). Similarly, in female mice, Cre⁺ mice showed reduced femur BMD and BMC compared to Cre⁻ mice longitudinally, with no differences in BMD or BMC of either the whole body or the spine (Figure 4B).

Deletion of $\alpha_2\delta_1$ in late-stage skeletal cells reduced cancellous bone in vivo at 10 wk in male mice

Hypothesizing that deletion of $\alpha_2\delta_1$ in osteocytes would impair cancellous bone development, longitudinal in vivo μCT measurements of the left proximal tibia were taken at 10 wk of age. In male Cre⁺ mice, deletion of $\alpha_2\delta_1$ in osteocytes did not alter trabecular spacing (Tb.Sp) but decreased BV/TV, trabecular number (Tb.N), and trabecular thickness (Tb.Th) ($P < .01$) in comparison to Cre⁻ male mice (Figure 5A). These differences in cancellous bone were not observed between female Cre⁺ and Cre⁻ mice at 10 wk of age, highlighting a sexually dimorphic effect during active skeletal growth (Figure 5B).

Reduced cancellous bone was alleviated in male mice, while female mice showed differences in cortical bone following skeletal maturity

To assess the impact of deleting $\alpha_2\delta_1$ in osteocytes on cancellous and cortical bone following skeletal maturity (20 wk of age), ex vivo μCT -derived measurements of the left proximal and midshaft tibiae, and left distal and midshaft femora were taken. Contrary to 10-wk in vivo μCT -derived measurements of the left proximal tibia, skeletally mature (20 wk old) male mice showed no differences in tibiae nor femoral μCT measurements (Supplementary Figures S1A and S2A). Female Cre⁺ mice continued to show no differences in cancellous bone measurements upon skeletal maturity, but cortical bone measurements of both the tibiae and femora revealed decreases in cortical thickness ($P < .01$), midshaft bone area (BA/TA), and polar moment of inertia (pMOI) ($P < .05$) in

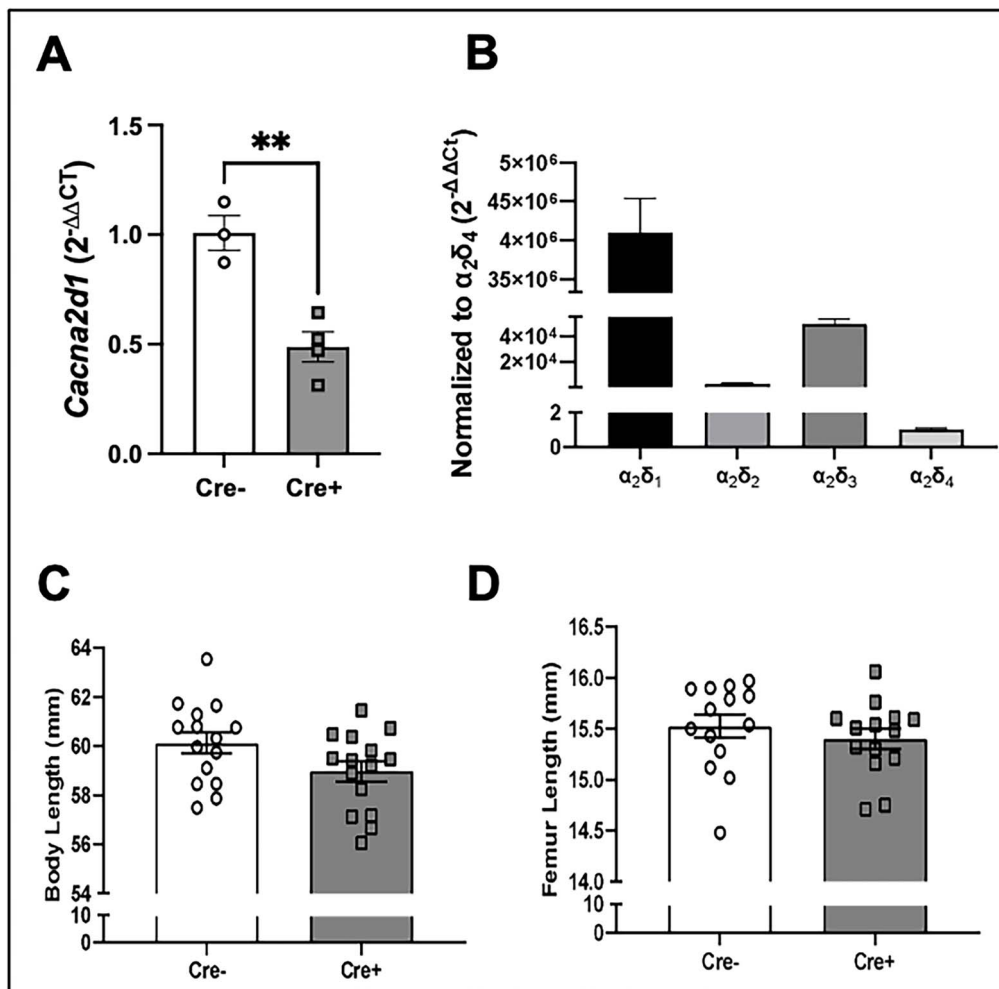


Figure 3. Deletion of $\alpha_2\delta_1$ in late-stage bone cells. (A) mRNA expression level of $\alpha_2\delta_1$ from cultured primary osteocytes. (B) mRNA expression levels of $\alpha_2\delta_{1-4}$ in IDG-SW3 cell-line following osteogenic differentiation. Body length (C) and femora length (D) were not different between Cre-negative and Cre-positive mice ($n = 15$ per group). **Significance was defined as a P value $< .01$. Values reported as means \pm SEM

comparison to female Cre $-$ mice (Supplementary Figures S1B and S2B).

Deletion of $\alpha_2\delta_1$ in late-stage skeletal cells resulted in impaired femoral strength in male mice

Three-point bending of femurs from 20-wk-old mice revealed a $\sim 15\%$ reduction in ultimate force ($P < .001$) and energy to failure ($P < .01$) in male Cre $+$ mice compared to Cre $-$ mice (Figure 6). No differences in femoral strength between genotypes were found in female mice (Figure 6).

Deletion of $\alpha_2\delta_1$ in late-stage skeletal cells negatively influenced osteoid formation and osteogenic gene expression

To assess osteoblast activity following deletion of $\alpha_2\delta_1$ in osteocytes, transcript levels were quantified by qPCR (Figure 7A), and histological analyses were carried out by staining for Von Kossa/McNeal (Figure 7B). Deletion of $\alpha_2\delta_1$ in osteocytes of male mice resulted in a 3-fold decrease in *Runx2* ($P < .05$), a 0.4-fold decrease in *Sp7* ($P < .01$), and a 0.6-fold decrease in *E11* ($P < .001$) mRNA levels. Cre $+$ male mice had a 2-fold increase in *Sost* ($P < .001$) mRNA (Figure 7A).

Deletion of $\alpha_2\delta_1$ in osteocytes did not alter relative osteoblast number nor relative osteoblast surface (Ob.S/BS). However, male Cre $+$ mice had significant reductions in osteoid area (O.Ar, $P < .001$), osteoid thickness (O.Th, $P < .05$), osteoid surface (OS/BS, $P < .05$), and relative osteoid volume (OV/BV) compared to Cre $-$ animals (Figure 7C). No changes in total osteocyte number nor osteocyte number normalized to bone area (N.Ocy/B.Ar) were observed in male Cre $+$ mice vs Cre $-$ animals (Figure 6C). Female Cre $+$ mice also showed a significant reduction (-30% , $P < .01$) in relative osteoid surface, but no changes in relative osteoblast number, osteoblast surface (Ob.S/BS), O.Ar, O.Th, osteocyte number, relative OV/BV, nor osteocyte number normalized to bone area (Figure 7D).

Deletion of $\alpha_2\delta_1$ in Dmp1-expressing cells did not alter histological measurements of osteoclast activity

Quantification of mRNA revealed a 35% decrease ($P < .05$) in *Acp5* (Trap), and a 56% decrease ($P < .01$) in *Tnfsf11b* (Opg) in Cre $+$ male mice compared to Cre $-$, with no changes in *Tnfsf11a* (RankL) (Figure 8B). Cre $+$ male mice had an increase in the ratio of RankL to Opg (3-fold, $P < .01$) compared to Cre $-$ animals (Figure 8A). Femurs from Cre $-$

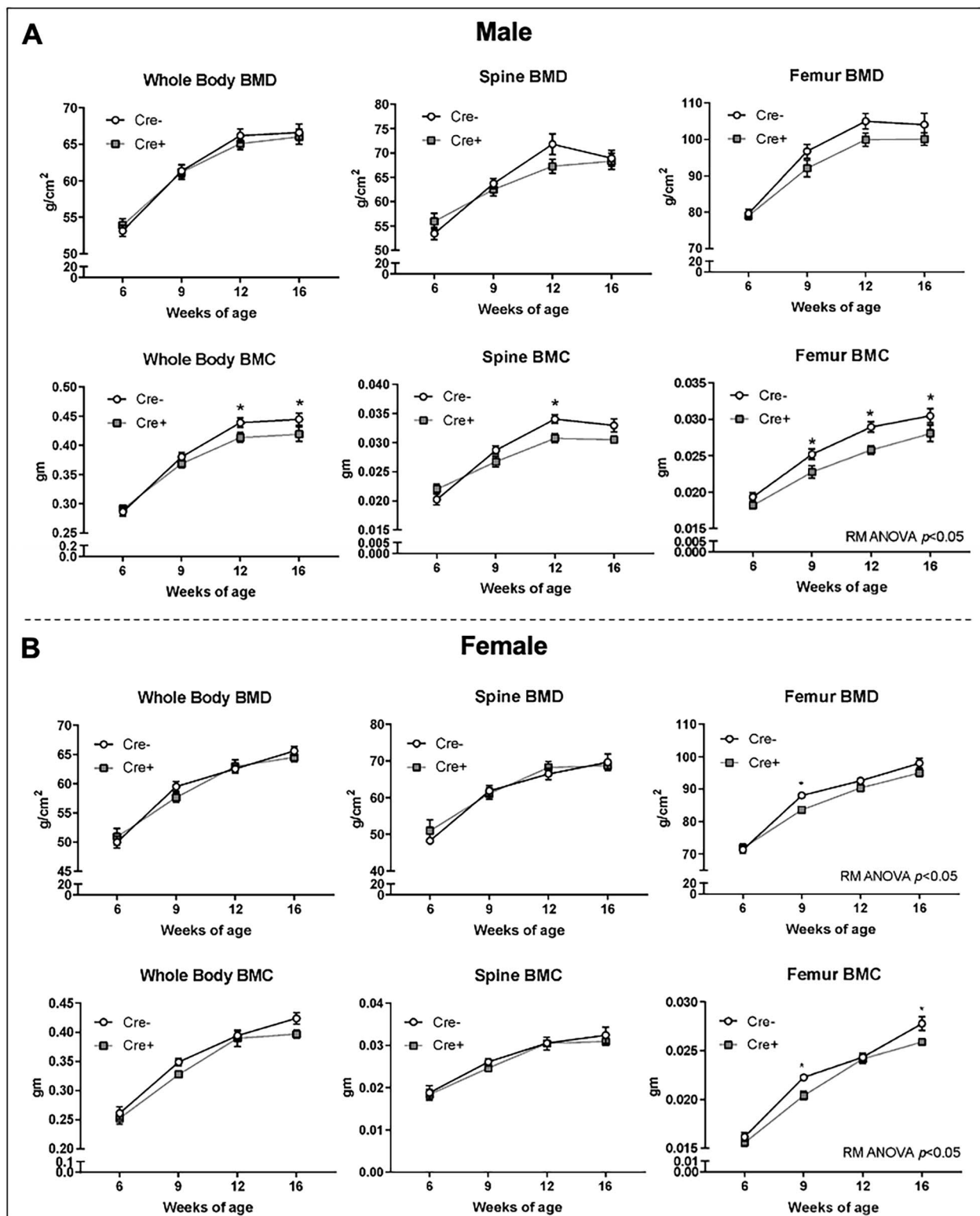


Figure 4. Longitudinal DXA BMD and BMC Measurements. DXA measurements of Cre-negative and Cre-positive male (A, $n = 15$) and female (B, $n = 11$) mice were taken every 3 wk and analyzed for whole body, lumbar spine (L2-L5), and right whole femur BMD and BMC. Longitudinal DXA data were tested for significance within sex and between Cre status using RM ANOVA. Sidak's multiple comparisons tests were used to assess differences at each timepoint within sex and between Cre status. *Significance was defined as a P value $< .05$. Values reported as means \pm SEM.

and Cre+ mice were sectioned and stained for TRAP to assess osteoclast activity (Figure 8B). Despite an increase in *Rankl/Opg* in Cre+ male mice, no differences were observed in osteoclast number, osteoclast surface (Oc.S/BS),

eroded perimeter (E.Pm), or eroded surface (ES/BS) in male Cre+ mice compared to Cre- animals (Figure 7C). In female mice, Cre+ animals had a 22% increase in ES/BS, but no changes in osteoclast number, Oc.S/BS, or E.Pm (Figure 8D).

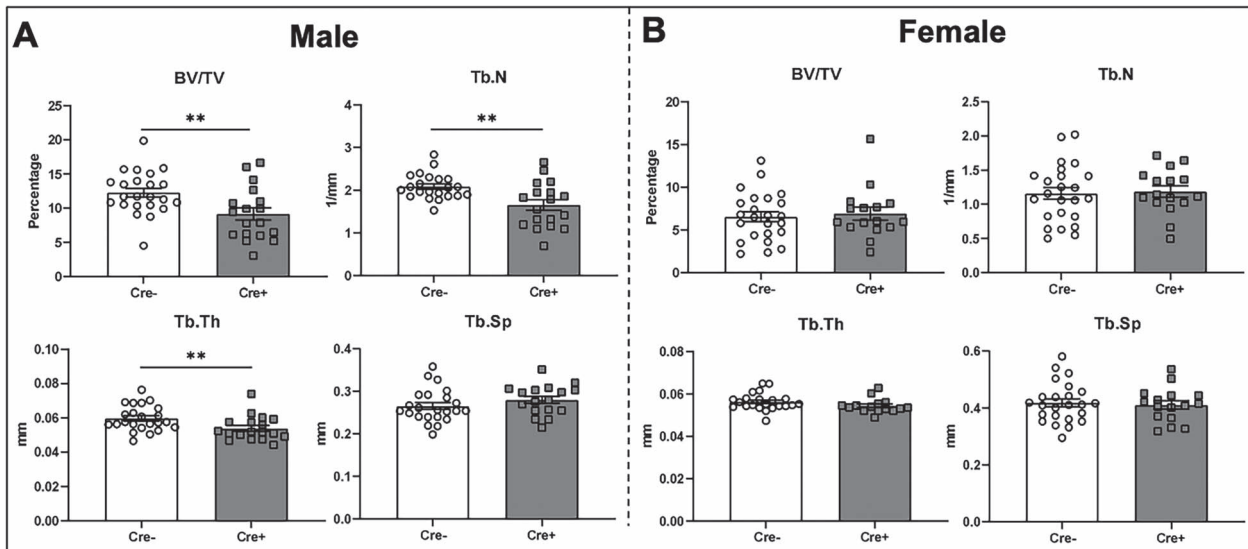


Figure 5. Ten week in vivo μ CT tibia trabecular measurements. In vivo μ CT-derived measurements of left proximal tibia cancellous bone from male (Cre-negative $n=24$; Cre-positive $n=18$) and female (Cre-negative $n=24$; Cre-positive $n=16$) mice at 10 wk of age. Independent t -tests were used to assess differences within sex and between Cre status. Significance was defined as a $P < .05$, ** $P < .01$. Values reported as means \pm SEM. Tibia trabecular bone volume fraction (BV/TV), Tb.N, Tb.Th, and Tb.Sp.

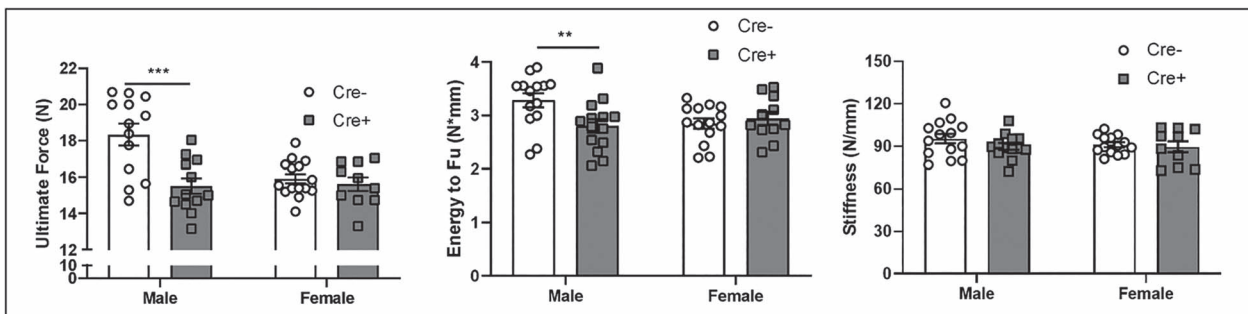


Figure 6. Mechanical properties of 20-wk-old femora. Three-point bending tests to failure were conducted on 20-wk-old whole femora from Cre-negative and Cre-positive male and female mice ($n=9-11$ per group). Differences in strength properties within sex and between Cre status were assessed using 2-way ANOVA. Significance was defined as a $P < .05$; ** $P < .01$, *** $P < .001$. Values reported as means \pm SEM.

Conditional deletion of $\alpha_2\delta_1$ in osteocytes reduced load-induced Ca^{2+} signaling in vivo

The MT3 of the mouse foot was loaded in vivo with simultaneous intravital imaging of osteocyte Ca^{2+} signaling to determine if $\alpha_2\delta_1$ regulates Ca^{2+} influx in osteocytes. Linear regression analysis compared strain dose–response curves to the number of osteocytes responding (Figure 9A and B). For both male and female animals, the slope of the response curve was unchanged; however, the y-intercept was lower for $G^{fl/fl}$ mice lacking $\alpha_2\delta_1$ compared to $G^{+/+}$ control mice (Figure 9A and B, $P < .05$). This downward shift of the response curve indicates that fewer osteocytes from $G^{fl/fl}$ mice responded to the mechanical input of a given strain magnitude compared to $G^{+/+}$ mice, indicating a reduction in osteocyte mechanosensitivity in the absence of $\alpha_2\delta_1$. Additionally, linear regression analysis was used to compare dose–response curves to the maximum intensity of responding cells as a function of strain (Figure 9C and D). For male mice, both the slope and intercept of Ca^{2+} signaling responses from $G^{fl/fl}$ mice were changed, representing a fundamental difference in how $\alpha_2\delta_1$ deficient male mice respond to mechanical loading (Figure 9C, $P < .05$). Female $G^{fl/fl}$ mice had a lower y-intercept but no

change in the response curve slope compared to $G^{+/+}$ mice (Figure 9D, $P < .05$).

Deletion of $\alpha_2\delta_1$ in osteocytes and late-stage osteoblasts impairs anabolic responses to loading in male mice

As our previous work found that $\alpha_2\delta_1$ is necessary for mechanosensation in osteocytes in culture,²⁸ and data from our metatarsal in vivo loading assays show that osteocytes lacking $\alpha_2\delta_1$ had altered mechanically induced Ca^{2+} signaling, we hypothesized that $\alpha_2\delta_1$ is necessary for anabolic responses to mechanical loading at the tissue-level. Thus, tibiae were loaded over a 10-d period using axial compression, and fluorochromes were injected to determine dynamic histomorphometry endpoints. Representative images of control (non-loaded) and loaded tibia from Cre– and Cre+ male mice show calcein and alizarin labeling in sections from the tibial mid-diaphysis (Figure 10A). Quantification of the labeled surfaces between control and loaded bones demonstrated significant increases in MS/BS, MAR, and BFR/BS in male Cre– mice. However, Cre+ male mice showed no significant increases in MS/BS, MAR, or BFR/BS

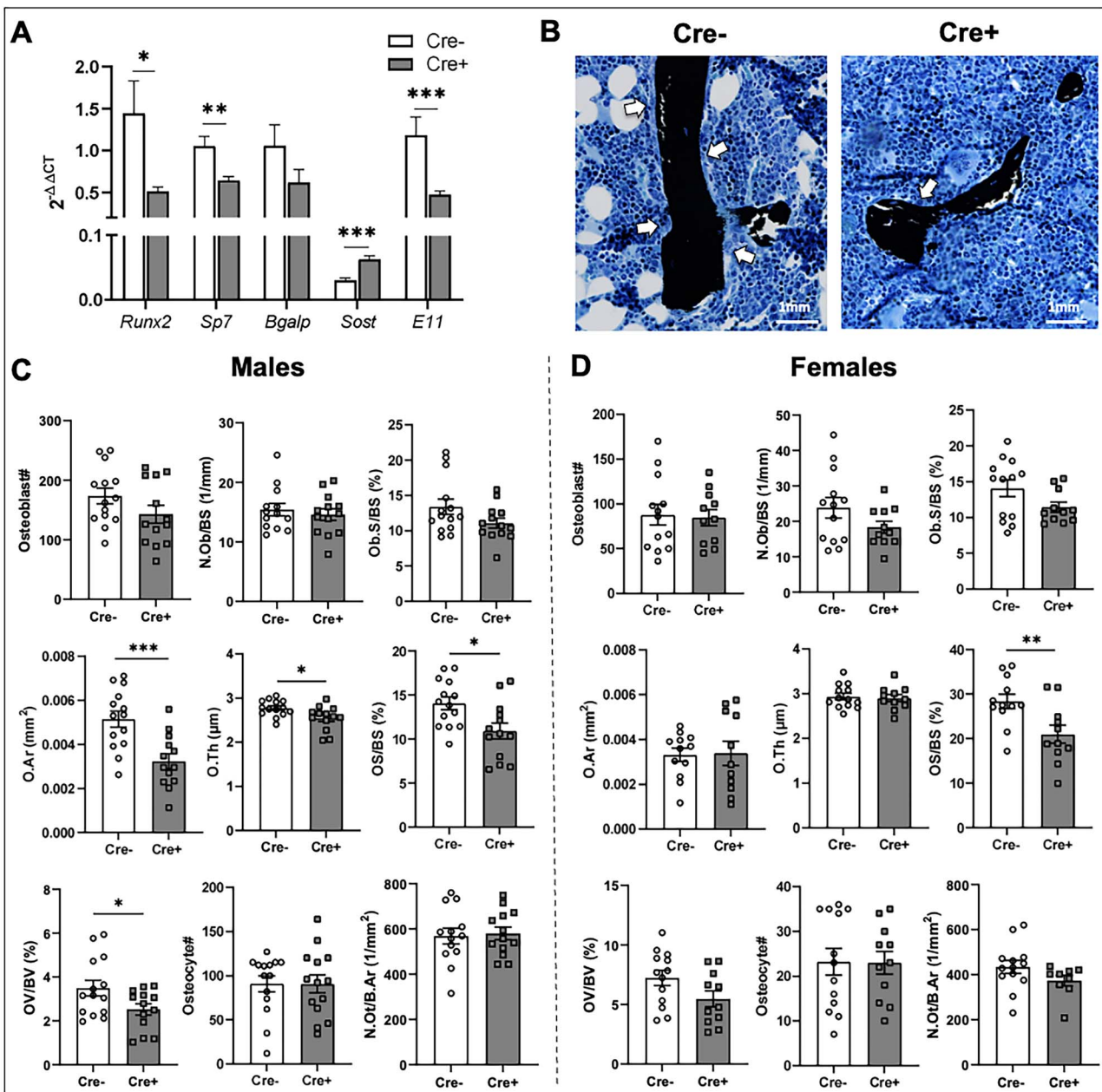


Figure 7. Histological analyses of VKM-stained sections of 20-wk-old femora. (A) Expression of osteoblast and osteocyte regulatory genes from 20-wk-old male mice including Runx2, osteocalcin (Bglap), Osterix (Sp7), sclerostin (Sost), and E11 were all normalized to Gapdh ($n = 11$ per group). (B) Representative images of distal femur sections from Cre-negative and Cre-Positive male mice stained with VKM. White arrows indicate osteoblasts on the bone surface. Histomorphometric quantification of osteoblast parameters from male (C) and female (D) mice including osteoblast number, osteoblast number relative to bone surface (N.Ob/BS), osteoblast surface normalized to bone surface (Ob.S/BS), osteocyte number, osteocyte number normalized to bone area (N.Ocy/B.Ar), O.Ar, O.Th, osteoid surface normalized to bone surface (OS/BS), and osteoid volume relative to bone volume (OV/BV) ($n = 11$ –14 per group). Data were tested for significance using unpaired Student's *t*-tests. Significance was defined as a $P < .05$, $P < .05^*$, $**P < .01$; $***P < .001$. Values reported as means \pm SEM.

following loading (Figure 10B, Supplementary Table S2). Notably, MS/BS was decreased (-87% , $P < .05$) in non-loaded Cre+ mice compared to non-loaded Cre- animals, further confirming decreased basal bone formation in mice lacking $\alpha_2\delta_1$ in osteocytes.

In female mice, MS/BS and BFR/BS were increased ($P < .05$) in Cre- mice with loading, showing an anabolic response in control animals. Female Cre+ mice had an increase in MS/BS after loading, but no significant changes in MAR or BFR/BS in response to axial compression (Figure 10C,

Supplementary Table S2), demonstrating some differential responses compared to males. Additionally, there were no differences in MS/BS in non-loaded female Cre+ mice compared to Cre- (Figure 10C, Supplementary Table S2), again supporting the sex-specific differences in bone formation responses seen with static histomorphometry measurements (Figure 7C and D).

To further quantify the contribution of $\alpha_2\delta_1$ to bone mechanotransduction and anabolic adaptation, μ CT measurements of the loaded (right) tibia were normalized to the

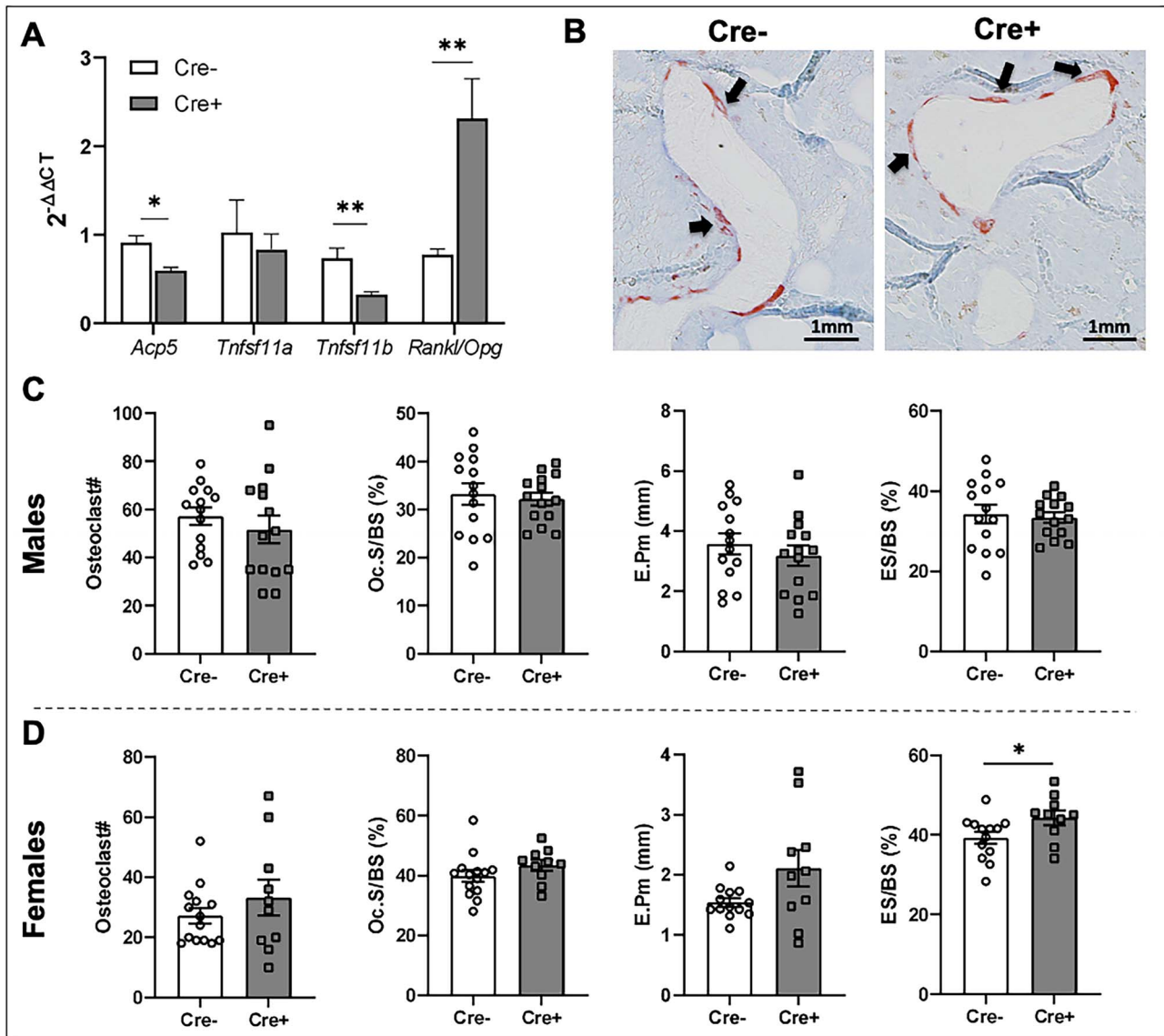


Figure 8. Histomorphometric analyses of TRAP-stained sections of 20-wk-old male femora. (A) Expression of osteoclast regulatory genes from 20-wk-old male mice including *Acp5* (TRAP), *Tnfsf11* (RankL), *Tnfsf11b* (Opg), and the ratio of RankL/Opg were all normalized to *Gapdh* ($n = 11$ per group). (B) Representative images of distal femur sections from Cre-negative and Cre-positive male mice stained for TRAP. Arrows indicate multinucleated osteoclasts stained crimson/red. (C) Histomorphometric quantification of osteoclast parameters from male (C) and female (D) mice including osteoclast number, osteoclast surface normalized to total bone surface (Oc.S/BS), E.Pm, and eroded surface normalized to total bone surface (ES/BS) ($n = 11$ –14 per group). Data were tested for significance using unpaired Student's *t*-tests. Significance was defined as a $P < .05$, $P < 0.05^*$, $**P < 0.01$. Values reported as means \pm SEM.

unloaded contralateral limb to generate delta values (loaded—unloaded, Figure 10D). Male Cre[−] mice showed a greater increase in delta tibial cortical BMD ($P < .01$) compared to Cre⁺ animals, but no differences in vBMD at the midshaft or cortical thickness were found. For female mice, no differences in change of cortical BMD or volumetric BMD (vBMD) at the midshaft were observed; however, Cre⁺ mice had a greater increase in delta cortical bone thickness ($P < .01$) compared to Cre[−] mice.

Discussion

The ability of bone to respond and adapt to mechanical force is essential for the preservation of bone health.⁴⁶ As such, conditions that lead to decreased skeletal loading or

disorders that impair bone mechanosensitivity can reduce BMD, increase fracture risk, and thus diminish the quality of life.^{1–3} The primary aim of this study was to determine the effects of deleting the $\alpha_2\delta_1$ auxiliary subunit in osteocytes on skeletal development and load-induced bone formation, as no other work has examined the function of $\alpha_2\delta_1$ in osteocytes in vivo.

Deletion of $\alpha_2\delta_1$ in osteocytes and late-stage osteoblasts only moderately affected longitudinal measurements of bone quantity during skeletal development. Due to its proposed role in mechanotransduction and that mechanical loading is important for skeletal growth and development,^{7–9} we anticipated deletion of $\alpha_2\delta_1$ in osteocytes and late-stage osteoblasts would result in a similar osteopenia phenotype to that seen in mice with global deletion of $\alpha_2\delta_1$ or Loss

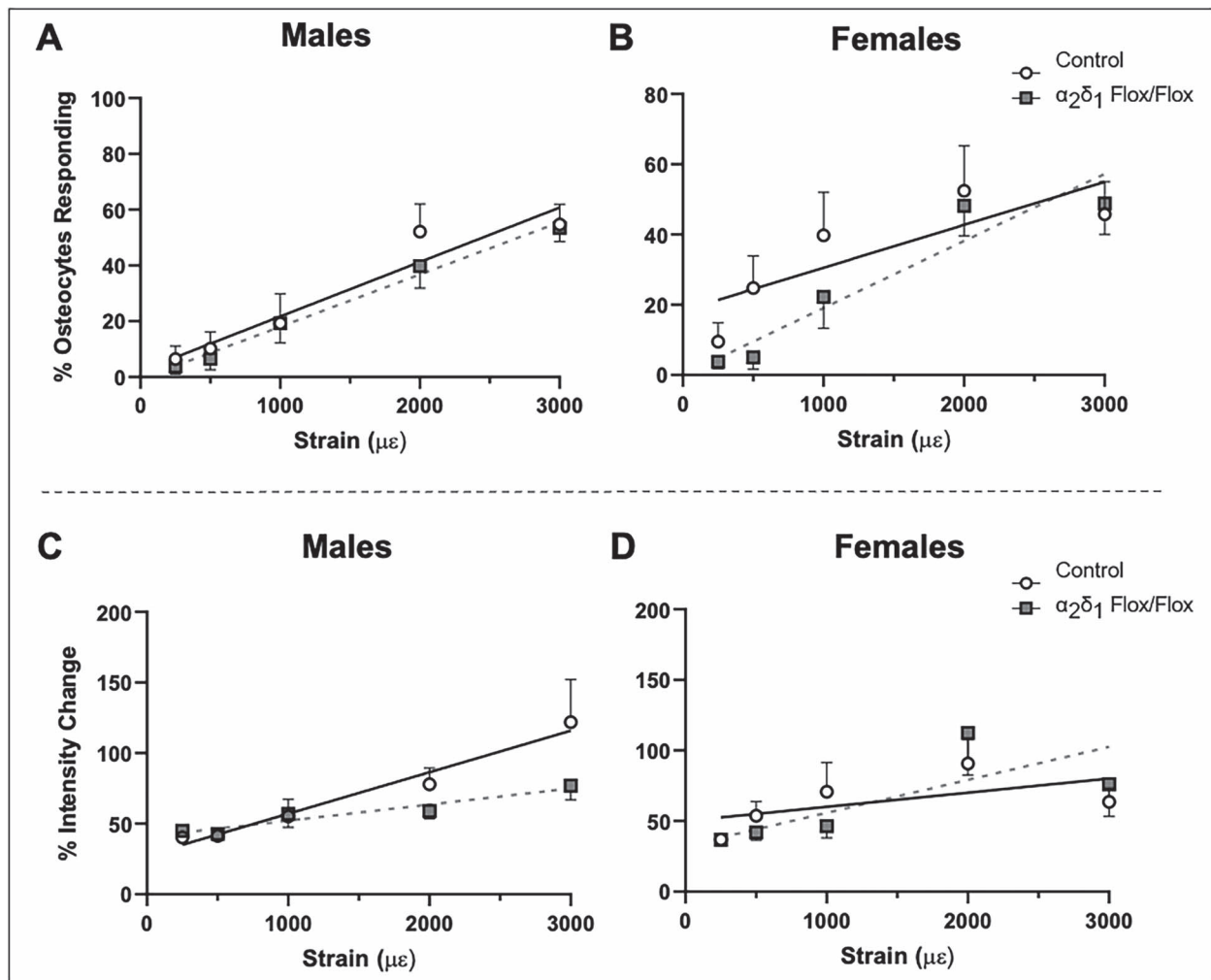


Figure 9. Linear regression analyses of calcium responses following in vivo MT3 loading reveal decreases in osteocyte mechanosensitivity. (A and B) Percentages of Ca^{2+} signaling osteocytes increased with increasing strain levels in male and female mice, revealing a similar linear relationship between the number of cells responding for both $G^{+/+}$ and $G^{fl/fl}$ male and female mice ($P > .05$). However, the y-intercept for $G^{fl/fl}$ male mice ($P = .001$) and $G^{fl/fl}$ female mice ($P = .0006$) decreased in comparison to $G^{+/+}$ animals, indicating a decrease in osteocyte mechanosensitivity. (C and D) Maximum intensity change among responding cells of $G^{+/+}$ and $G^{fl/fl}$ male and female mice. The relationship between maximum response intensity and strain magnitude (ie, slope) increased in $G^{+/+}$ male mice; however, the y-intercept and slope were fundamentally altered in $G^{fl/fl}$ male mice ($P = .014$). The linear relationship between maximum response intensity and strain magnitude was unchanged in female mice; however, the y-intercept was decreased ($P = .005$) in $G^{fl/fl}$ female mice.

of the auxiliary $\alpha_2\delta_1$ voltage sensitive calcium channel subunit impairs bone formation and anabolic responses to mechanical loading low-density lipoprotein (LDL) receptor-related protein (LRP5).⁴⁷ However, deletion of $\alpha_2\delta_1$ in osteocytes only moderately affected bone morphology with lower longitudinal femur BMC. Impairments in cancellous bone were observed in male mice at 10 wk of age, but these differences dissipated upon skeletal maturity. Although DMP1-Cre mediated deletion of $\alpha_2\delta_1$ resulted in relatively small differences in overall bone structure compared to control mice, the lack of $\alpha_2\delta_1$ in osteocytes impaired anabolic responses to mechanical loading, which aligns well with the proposed function of $\alpha_2\delta_1$ in mechanotransduction. As such, this moderate basal skeletal phenotype coincides with previous publications where, despite modest morphological changes in bone, robust anabolic differences are apparent when presented with a challenge. Two examples of this robust anabolic response include the global *Nmp4* KO mice⁴⁸ and mice with conditional deletion of *Nmp4*

(DMP-cre).⁴⁹ Both models showed moderate effects on basal bone quantity measurements, but exhibited dramatic increases in BFRs following PTH treatment, beyond that of controls or heterozygous mice. Similarly, marginal differences in vertebral BMD were observed in mice overexpressing sclerostin using the DMP1 promoter, but when challenged with ulnar loading, these mice showed significant reductions in BFRs.⁵⁰ As such, it is not uncommon to observe a disparity between basal skeletal phenotype and phenotypes that manifest upon meeting an anabolic threshold, as in the current study, or over time with age. Therefore, additional analyses in post-weaning and in aged mice could provide further insights into the extent of the auxiliary subunit's role in the developmental process.

Deletion of $\alpha_2\delta_1$ in osteocytes and late-stage osteoblasts resulted in impaired load-induced bone formation in response to tibial axial compression in male mice. These diminished mechanosensitive responses were further highlighted by decreased adaptive responses in cortical bone, where control mice showed greater increases in tibial cortical

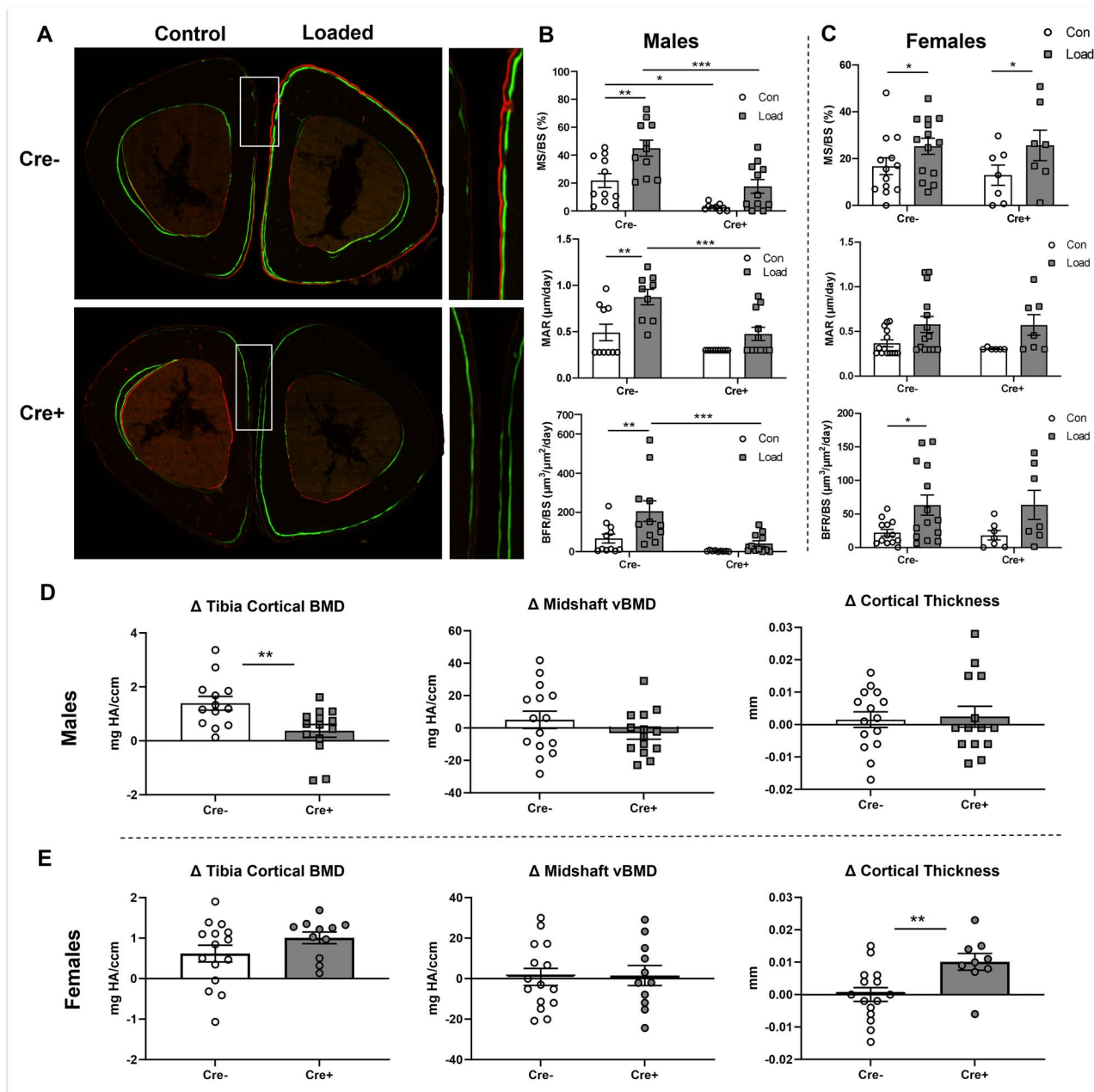


Figure 10. Axial tibial loading revealed differences in bone formation. Strain-matched peak forces were applied to the right tibia of 20-wk-old Cre-negative Cre-positive male and female mice. (A) Representative images of control (non-loaded) and loaded tibia from Cre-negative and Cre+ male mice (female images in supp. materials). (B) MS/BS, MAR, and BFR/BS of Cre-negative and Cre-positive male and female mice ($N=11$). (C) μCT -derived cortical bone responses following tibial axial compression normalized to unloaded contralateral control limb of Cre-negative and Cre-positive male and female mice ($N=11-15$). Differences in loading and Cre status were assessed using MANOVA. Significance was defined as a $P < .05^*$; $**P < .01$; $***P < .001$. Values reported as means \pm SEM.

BMD in response to loading vs mice lacking $\alpha_2\delta_1$ in osteocytes. The observed differences in tissue level responses to anabolic loading could be explained by functions of VSCCs independent of $\alpha_2\delta_1$. To interrogate whether $\alpha_2\delta_1$ directly regulates mechanically induced Ca^{2+} signaling responses, we used intravital fluorescent imaging to observe load-induced osteocyte Ca^{2+} influx in vivo, in real-time. We found that the relationship between load magnitude and the number of responsive cells was shifted downward in mice lacking $\alpha_2\delta_1$ in osteocytes, indicating a decrease in overall mechanosensitivity. Furthermore, deletion of $\alpha_2\delta_1$

in osteocytes decreased maximal Ca^{2+} signal intensity in response to mechanical loading. As such, the impaired mechanical response following tibial loading of mice lacking $\alpha_2\delta_1$ in osteocytes is likely related to changes in osteocyte mechanosensitivity, as indicated by Ca^{2+} signaling activation. These results demonstrate the function of VSCCs in osteocyte mechanotransduction^{28,51} and the regulatory role of its auxiliary subunit $\alpha_2\delta_1$.

Although numerous studies have shown that VSCCs are necessary for anabolic responses of bone to mechanical input, the mechanism by which VSCCs are activated by force to

initiate Ca^{2+} influx remained unclear. The current prevailing theory is that upon mechanical stimulation, nearby mechanosensitive Ca^{2+} channels open and induce a small, localized influx of Ca^{2+} ⁵², which produces a negative membrane potential. This depolarization of the cell membrane is then sensed by VSCCs causing the gating of its α_1 pore-forming subunit and the flooding of Ca^{2+} into the intracellular space.¹⁵ In this study, we showed that the VSCC auxiliary subunit $\alpha_2\delta_1$ is necessary for the anabolic responses to mechanical loading. Deletion of $\alpha_2\delta_1$ in osteocytes impaired load-induced (1) Ca^{2+} influx in vivo, (2) BFRs, and (3) adaptive skeletal responses. Previous work has shown that $\alpha_2\delta_1$ facilitates trafficking of the α_1 pore-forming subunit to the plasma membrane.^{28,53} Therefore, one possible explanation for our findings is that osteocytes lacking $\alpha_2\delta_1$ have fewer mechanoresponsive VSCCs. Alternatively, the extracellular location of $\alpha_2\delta_1$ interacts with the pericellular matrix, enabling the direct activation of VSCCs through fluid-shear drag forces. The mechanisms by which mechanical forces are directly transmitted through $\alpha_2\delta_1$ to open VSCCs are supported by our recent findings that $\alpha_2\delta_1$ binds PLN, a large heparan sulfate proteoglycan.²⁵ We have previously shown that PLN is a component of the tethering elements that span the osteocyte pericanalicular space²⁶ and regulate mechanosensation²⁷ and ultrastructure.⁵⁴ As PLN deficient mice have impaired Ca^{2+} signaling responses and $\alpha_2\delta_1$ binds strongly to PLN,²⁵ the direct physical connection of PLN tethers to VSCCs likely influences Ca^{2+} gating-kinetics and therefore load-induced anabolic responses.

Our data demonstrate that deletion of $\alpha_2\delta_1$ in late-stage skeletal cells reduced histological measurements of osteoid. Loss of $\alpha_2\delta_1$ in osteocytes and late-stage osteoblasts in male mice did not influence total osteoblast nor osteocyte number, but instead decreased O.Ar, O.Th, osteoid volume, and osteoid surface relative to controls. Female mice showed a similar reduction in relative osteoid surface in comparison to controls despite a lack of change in osteoblast and osteocyte number. These reductions in histological measurements of osteoid may result from decreased osteoblast activity and/or an acceleration of bone mineralization. However, without bone formation measurements on the same bone surface, it is not possible to determine which one of the two is the cause for the observed phenotype following deletion of $\alpha_2\delta_1$ in late-stage skeletal cells. Nevertheless, based on the lack of an increase in MAR following tibial loading and the decreased production of osteogenic genes (*E11*, *Runx2*, *Sp7*, and *Bglap*), the decrease in osteoid measurements observed in cancellous bone is consistent with reduced osteoblast activity. Further studies will need to be conducted to confirm this impairment in osteoblast activity.

The impairment in femoral strength in male mice lacking $\alpha_2\delta_1$ in osteocytes and late-stage osteoblasts is likely due to a combination of multiple factors. In addition to a decrease in femoral bone content, mechanosensitivity, and osteogenic gene expression, the reduction in osteoid formation in Cre + male mice could collectively contribute to the impairment in femoral strength. Furthermore, previous work has shown that PLN is necessary for maintaining the open, unmineralized pericanalicular space.²⁶ Given our recent work found that $\alpha_2\delta_1$ tightly binds to PLN,²⁵ it is plausible that deletion of $\alpha_2\delta_1$ in osteocytes disrupts this connection, altering the osteocyte's pericanalicular space. Ongoing work is currently examining how $\alpha_2\delta_1$ influences lacunocanalicular morphology, which may contribute to the reduction in femoral

strength observed in these male mice. Interestingly, despite a reduction in femoral BMD & BMC, and decreased cortical thickness and pMOI, female mice lacking $\alpha_2\delta_1$ in osteocytes showed no differences in femoral strength in comparison to controls. Therefore, additional work is needed to delineate how $\alpha_2\delta_1$ produced by osteocytes alters bone matrix properties and canalicular dimensions, and how sex influences their contribution to the phenotype.

Deletion of the $\alpha_2\delta_1$ subunit in late-stage skeletal cells revealed sexual dimorphism in skeletal morphology, mechanical properties, in vivo Ca^{2+} signaling responses, and anabolic responses to mechanical loading, suggesting a role of sex steroids in the regulation of VSCC-mediated skeletal development and mechanotransduction. Estrogen has a significant role in bone cell remodeling, decreasing osteoclast activity while increasing osteoblast differentiation and the mechanosensitivity of both osteoblasts and osteocytes.⁵⁵⁻⁵⁷ Decreases in circulating estrogen or loss of its nuclear receptors ($\text{ER}\alpha$ and $\text{ER}\beta$) can increase osteoclast activity, decrease osteoblast differentiation, and inhibit load-induced anabolic responses.^{55,58,59} Thus, the observed sex-specific differences in Ca^{2+} signaling and mechanical responses may result from the influence of estrogen on Ca^{2+} influx in osteocytes.^{37,60-62}

The strengths of this work include the targeted deletion of $\alpha_2\delta_1$ in late-stage skeletal cells to determine the bone-specific consequences of $\alpha_2\delta_1$ deletion. Furthermore, the use of intravital imaging allowed us to examine the function of $\alpha_2\delta_1$ in osteocytes on Ca^{2+} influx in live mice subjected to mechanical loading in real time. These data support the conclusion that $\alpha_2\delta_1$ regulates Ca^{2+} influx in response to mechanical force, which is necessary for the anabolic responses of bone to loading. Although we examined the responses of both male and female mice, the mechanisms related to the sex differences remain unclear and are a worthy subject for future investigation. Additionally, though our results showed that deletion of $\alpha_2\delta_1$ in osteocytes decreased load induced Ca^{2+} influx in osteocytes in vivo, additional studies are needed to determine the specific intracellular signaling pathways influenced by $\alpha_2\delta_1$ deletion and their contribution to the observed phenotype.

In summary, mice lacking the $\alpha_2\delta_1$ auxiliary VSCC subunit in osteocytes and late-stage osteoblasts exhibit decreased mechanosensitivity. These results highlight the function $\alpha_2\delta_1$ and its ability to influence skeletal adaptation in response to mechanical loading. Although there were no differences in osteoblast or osteocyte number, deletion of $\alpha_2\delta_1$ in osteocytes and late stage osteoblasts decreased osteoid and femoral strength which may directly or indirectly be related to decreases in mechanosensitivity and alterations in osteogenic gene expression. *Cacna2d1^{fl/fl}*, Cre + females showed only partial inhibition of load-induced bone formation, suggesting sex-specific differences in osteocyte mechanosensitivity and mechanotransduction pathways. Collectively, these data show that the auxiliary $\alpha_2\delta_1$ subunit mediates the mechanical forces regulating VSCC-mediated Ca^{2+} influx in osteocytes, providing a possible avenue for therapeutic intervention.

Author contributions

Christian S. Wright (Conceptualization, Data curation, Formal analysis, Resources, Writing—original draft, Writing—review & editing), Karl J. Lewis (Data curation, Formal analysis, Writing—review & editing),

Katelyn Semon (Data curation, Formal analysis, Writing—review & editing), Xin Yi (Data curation, Formal analysis, Writing—review & editing), Perla C. Reyes-Fernandez (Data curation, Formal analysis, Writing—review & editing), Katie Rust (Data curation, Formal analysis, Writing—review & editing), Matthew Prideaux (Data curation, Formal analysis, Writing—review & editing), Artur Schneider (Data curation, Writing—review & editing), Molly Pederson (Data curation, Writing—review & editing), Padmini Deosthale (Data curation, Writing—review & editing), Lilian I. Plotkin (Data curation, Formal analysis, Writing—review & editing), Julia M. Hum (Conceptualization, Data curation, Formal analysis, Writing—review & editing), Uma Sankar (Conceptualization, Data curation, Formal analysis, Writing—review & editing), Mary C. Farach-Carson (Conceptualization, Data curation, Formal analysis, Writing—original draft, Writing—review & editing), Alexander G. Robling (Conceptualization, Data curation, Formal analysis, Writing—review & editing), and William R. Thompson (Conceptualization, Data curation, Formal analysis, Writing—original draft, Writing—review & editing).

Supplementary material

Supplementary material is available at *Journal of Bone and Mineral Research* online.

Funding

This study was supported by 1F32AR074893-01 to C.S.W., 1R01AR074473-01 to W.R.T., UL1 TR001108 to W.R.T. and A.G.R., Veterans Research Administration Merit Award I10 1BX005154 to L.L.P., Marian University Faculty Development Grants, Indiana University Research Support Funds Grant.

Conflicts of interest

None declared.

Data availability

The data underlying this article will be shared on reasonable request to the corresponding author.

References

- Alexandre C, Vico L. Pathophysiology of bone loss in disuse osteoporosis. *Joint Bone Spine*. 2011;78(6):572–576. <https://doi.org/10.1016/j.jbspin.2011.04.007>.
- Krasnoff J, Painter P. The physiological consequences of bed rest and inactivity. *Adv Renal Replace Ther*. 1999;6(2):124–132. [https://doi.org/10.1016/S1073-4449\(99\)70030-0](https://doi.org/10.1016/S1073-4449(99)70030-0).
- Brauer CA, Coca-Perrillon M, Cutler DM, Rosen AB. Incidence and mortality of hip fractures in the United States. *JAMA*. 2009;302(14):1573–1579. <https://doi.org/10.1001/jama.2009.1462>.
- Hansen DPP, Pyenson B. *Medicare Cost of Osteoporotic Fractures – 2021 Updated Report*. Milliman Research Report, Seattle, WA: National Osteoporosis Foundation; 2021.
- Niziolek PJ, Warman ML, Robling AG. Mechanotransduction in bone tissue: The A214V and G171V mutations in Lrp5 enhance load-induced osteogenesis in a surface-selective manner. *Bone*. 2012;51(3):459–465. <https://doi.org/10.1016/j.bone.2012.05.023>.
- Yeh EJ, Gitlin M, Sorio F, McCloskey E. Estimating the future clinical and economic benefits of improving osteoporosis diagnosis and treatment among postmenopausal women across eight European countries. *Arch Osteoporos*. 2023;18(1):68. <https://doi.org/10.1007/s11657-023-01230-0>.

- Thompson WR, Rubin CT, Rubin J. Mechanical regulation of signaling pathways in bone. *Gene*. 2012;503(2):179–193. <https://doi.org/10.1016/j.gene.2012.04.076>.
- Karlsson MK, Johnell O, Obrant KJ. Bone mineral density in weight lifters. *Calcif Tissue Int*. 1993;52(3):212–215. <https://doi.org/10.1007/BF00298721>.
- Turner CH, Robling AG. Exercise as an anabolic stimulus for bone. *Curr Pharm Design*. 2004;10(21):2629–2641. <https://doi.org/10.2174/1381612043383755>.
- Warden SJ, Thompson WR. Become one with the force: optimising mechanotherapy through an understanding of mechanobiology. *Br J Sports Med*. 2017;51(13):989–990. <https://doi.org/10.1136/bjsports-2017-097634>.
- Zigdon-Giladi H, Rudich U, Michaeli Geller G, Evron A. Recent advances in bone regeneration using adult stem cells. *World J Stem Cells*. 2015;7(3):630–640. <https://doi.org/10.4252/wjsc.v7.i3.630>.
- Bonewald LF. The amazing osteocyte. *J Bone Miner Res*. 2011;26(2):229–238. <https://doi.org/10.1002/jbmr.320>.
- Ajubi NE, Klein-Nulend J, Alblas MJ, Burger EH, Nijweide PJ. Signal transduction pathways involved in fluid flow-induced PGE(2) production by cultured osteocytes. *Am J Physiol Endocrinol Metab*. 1999;276(1):E171–E178. <https://doi.org/10.1152/ajpendo.1999.276.1.E171>.
- Hung CT, Allen FD, Pollack SR, Brighton CT. Intracellular Ca²⁺ stores and extracellular Ca²⁺ are required in the real-time Ca²⁺ response of bone cells experiencing fluid flow. *J Biomech*. 1996;29(11):1411–1417. [https://doi.org/10.1016/0021-9290\(96\)84536-2](https://doi.org/10.1016/0021-9290(96)84536-2).
- Wright CS, Robling AG, Farach-Carson MC, Thompson WR. Skeletal functions of voltage sensitive calcium channels. *Curr Osteoporos Rep*. 2021;19(2):206–221. <https://doi.org/10.1007/s11914-020-00647-7>.
- Li J, Zhao L, Ferries IK, et al. Skeletal phenotype of mice with a null mutation in Cav 1.3 L-type calcium channel. *J Musculoskelet Neuronal Interact*. 2010;10(2):180–187.
- Duriez J, Flautre B, Blary MC, Hardouin P. Effects of the calcium channel blocker nifedipine on epiphyseal growth plate and bone turnover: a study in rabbit. *Calcif Tissue Int*. 1993;52(2):120–124. <https://doi.org/10.1007/BF00308320>.
- Wen L, Wang Y, Wang H, et al. L-type calcium channels play a crucial role in the proliferation and osteogenic differentiation of bone marrow mesenchymal stem cells. *Biochem Biophys Res Commun*. 2012;424(3):439–445. <https://doi.org/10.1016/j.bbrc.2012.06.128>.
- Li J, Duncan RL, Burr DB, Turner CH. L-type calcium channels mediate mechanically induced bone formation in vivo. *J Bone Miner Res Off J Am Soc Bone Miner Res*. 2002;17(10):1795–1800. <https://doi.org/10.1359/jbmr.2002.17.10.1795>.
- Ridings JE, Palmer AK, Davidson EJ, Baldwin JA. Prenatal toxicity studies in rats and rabbits with the calcium channel blocker diproterverine. *Reprod Toxicol*. 1996;10(1):43–49. [https://doi.org/10.1016/0890-6238\(95\)02017-9](https://doi.org/10.1016/0890-6238(95)02017-9).
- Li J, Duncan RL, Burr DB, Gattone VH, Turner CH. Parathyroid hormone enhances mechanically induced bone formation, possibly involving L-type voltage-sensitive calcium channels. *Endocrinology*. 2003;144(4):1226–1233. <https://doi.org/10.1210/en.2002-220821>.
- Dolphin AC. Voltage-gated calcium channels and their auxiliary subunits: physiology and pathophysiology and pharmacology. *J Physiol*. 2016;594(19):5369–5390. <https://doi.org/10.1113/JP272262>.
- Jones LP, Wei SK, Yue DT. Mechanism of auxiliary subunit modulation of neuronal alpha1E calcium channels. *J Gen Physiol*. 1998;112(2):125–143. <https://doi.org/10.1085/jgp.112.2.125>.
- Wakamori M, Mikala G, Mori Y. Auxiliary subunits operate as a molecular switch in determining gating behaviour of the unitary N-type Ca²⁺ channel current in *Xenopus* oocytes. *J Physiol*. 1999;517(3):659–672. <https://doi.org/10.1111/j.1469-7793.1999.0659s.x>.

25. Reyes, Fernandez PC, Wright CS, Masterson AN, et al. Gabapentin disrupts binding of perlecan to the alpha(2)delta(1) voltage sensitive calcium channel subunit and impairs skeletal mechanosensation. *Biomolecules*. 2022;12(12):1857. <https://doi.org/10.3390/biom12121857>.
26. Thompson WR, Modla S, Grindel BJ, et al. Perlecan/Hspg2 deficiency alters the pericellular space of the lacunocanalicular system surrounding osteocytic processes in cortical bone. *J Bone Miner Res Off J Am Soc Bone Miner Res*. 2011;26(3):618–629. <https://doi.org/10.1002/jbmr.236>.
27. Wang B, Lai X, Price C, et al. Perlecan-containing pericellular matrix regulates solute transport and mechanosensing within the osteocyte lacunar-canalicular system. *J Bone Miner Res Off J Am Soc Bone Miner Res*. 2014;29(4):878–891. <https://doi.org/10.1002/jbmr.2105>.
28. Thompson WR, Majid AS, Czymbek KJ, et al. Association of the $\alpha 2\delta 1$ subunit with Cav3.2 enhances membrane expression and regulates mechanically induced ATP release in MLO-Y4 osteocytes. *J Bone Miner Res*. 2011;26(9):2125–2139. <https://doi.org/10.1002/jbmr.437>.
29. Kim H, Kim M, Im SK, Fang S. Mouse Cre-LoxP system: general principles to determine tissue-specific roles of target genes. *Lab Anim Res*. 2018;34(4):147–159. <https://doi.org/10.5625/lar.2018.34.4.147>.
30. Park J, Yu YP, Zhou CY, et al. Central Mechanisms Mediating Thrombospondin-4-induced Pain States. *J Biol Chem*. 2016;291(25):13335–13348. <https://doi.org/10.1074/jbc.M116.723478>.
31. Lu Y, Xie Y, Zhang S, Dusevich V, Bonewald LF, Feng JQ. DMP1-targeted Cre expression in odontoblasts and osteocytes. *J Dent Res*. 2007;86(4):320–325. <https://doi.org/10.1177/154405910708600404>.
32. Chen TW, Wardill TJ, Sun Y, et al. Ultra-sensitive fluorescent proteins for imaging neuronal activity. *Nature*. 2013;499(7458):295–300. <https://doi.org/10.1038/nature12354>.
33. Lewis KJ, Frikha-Benayed D, Louie J, et al. Osteocyte calcium signals encode strain magnitude and loading frequency in vivo. *Proc Natl Acad Sci U S A*. 2017;114(44):11775–11780. <https://doi.org/10.1073/pnas.1707863114>.
34. Woo SM, Rosser J, Dusevich V, Kalajzic I, Bonewald LF. Cell line IDG-SW3 replicates osteoblast-to-late-osteocyte differentiation in vitro and accelerates bone formation in vivo. *J Bone Miner Res Off J Am Soc Bone Miner Res*. 2011;26(11):2634–2646. <https://doi.org/10.1002/jbmr.465>.
35. Kedlaya R, Veera S, Horan DJ, et al. Sclerostin inhibition reverses skeletal fragility in an Lrp5-deficient mouse model of OPGG syndrome. *Sci Transl Med*. 2013;5(211):ra158. <https://doi.org/10.1126/scitranslmed.3006627>.
36. Boussein ML, Boyd SK, Christiansen BA, Gulberg RE, Jepsen KJ, Muller R. Guidelines for assessment of bone microstructure in rodents using micro-computed tomography. *J Bone Miner Res Off J Am Soc Bone Miner Res*. 2010;25(7):1468–1486. <https://doi.org/10.1002/jbmr.141>.
37. Lewis KJ, Cabahug-Zuckerman P, Boorman-Padgett JF, et al. Estrogen depletion on In vivo osteocyte calcium signaling responses to mechanical loading. *Bone*. 2021;152:116072. <https://doi.org/10.1016/j.bone.2021.116072>.
38. Cui Y, Niziolek PJ, MacDonald BT, et al. Lrp5 functions in bone to regulate bone mass. *Nat Med*. 2011;17(6):684–691. <https://doi.org/10.1038/nm.2388>.
39. Turner CH, Burr DB. Basic biomechanical measurements of bone: a tutorial. *Bone*. 1993;14(4):595–608. [https://doi.org/10.1016/8756-3282\(93\)90081-K](https://doi.org/10.1016/8756-3282(93)90081-K).
40. Thompson WR, Yen SS, Uzer G, et al. LARG GEF and ARHGAP18 orchestrate RhoA activity to control mesenchymal stem cell lineage. *Bone*. 2018 Feb;107:172–180. <https://doi.org/10.1016/j.bone.2017.12.001>.
41. Williams JN, Kambrath AV, Patel RB, et al. Inhibition of CaMKK2 enhances fracture healing by stimulating Indian Hedgehog signaling and accelerating endochondral ossification. *J Bone Miner Res Off J Am Soc Bone Miner Res*. 2018;33(5):930–944. <https://doi.org/10.1002/jbmr.3379>.
42. Schenk RO, Herrmann W. Preparation of calcified tissues for light microscopy. In: Dickson G, ed. *Methods of Calcified Tissue Preparation*. Amsterdam: Elsevier; 1984:1–56.
43. Erlebacher A, Derynck R. Increased expression of TGF-beta 2 in osteoblasts results in an osteoporosis-like phenotype. *J Cell Biol*. 1996;132(1):195–210. <https://doi.org/10.1083/jcb.132.1.195>.
44. Dempster DW, Compston JE, Drezner MK, et al. Standardized nomenclature, symbols, and units for bone histomorphometry: a 2012 update of the report of the ASBMR Histomorphometry Nomenclature Committee. *J Bone Miner Res Off J Am Soc Bone Miner Res*. 2013;28(1):2–17. <https://doi.org/10.1002/jbmr.1805>.
45. Hoaglin DC, Iglewicz B. Fine-tuning some resistant rules for outlier labeling. *J Am Stat Assoc*. 1987;82(400):1147–1149. <https://doi.org/10.1080/01621459.1987.10478551>.
46. Thompson WR, Scott A, Loghmani MT, Ward SR, Warden SJ. Understanding mechanobiology: physical therapists as a force in mechanotherapy and musculoskeletal regenerative rehabilitation. *Phys Ther*. 2016;96(4):560–569. <https://doi.org/10.2522/ptj.20150224>.
47. Sawakami K, Robling AG, Ai M, et al. The Wnt co-receptor LRP5 is essential for skeletal mechanotransduction but not for the anabolic bone response to parathyroid hormone treatment. *J Biol Chem*. 2006;281(33):23698–23711. <https://doi.org/10.1074/jbc.M601000200>.
48. Robling AG, Childress P, Yu J, et al. Nmp4/CIZ suppresses parathyroid hormone-induced increases in trabecular bone. *J Cell Physiol*. 2009;219(3):734–743. <https://doi.org/10.1002/jcp.21717>.
49. Atkinson EG, Adaway M, Horan DJ, et al. Conditional loss of Nmp4 in mesenchymal stem progenitor cells enhances PTH-induced bone formation. *J Bone Miner Res Off J Am Soc Bone Miner Res*. 2023;38(1):70–85. <https://doi.org/10.1002/jbmr.4732>.
50. Tu X, Rhee Y, Condon KW, et al. Lost downregulation and local Wnt signaling are required for the osteogenic response to mechanical loading. *Bone*. 2012;50(1):209–217. <https://doi.org/10.1016/j.bone.2011.10.025>.
51. Brown GN, Leong PL, Guo XE. T-Type voltage-sensitive calcium channels mediate mechanically-induced intracellular calcium oscillations in osteocytes by regulating endoplasmic reticulum calcium dynamics. *Bone*. 2016 Jul;88:56–63. <https://doi.org/10.1016/j.bone.2016.04.018>.
52. Qin L, Liu W, Cao H, Xiao G. Molecular mechanosensors in osteocytes. *Bone Res*. 2020;8(1):23. <https://doi.org/10.1038/s41413-020-0099-y>.
53. Dolphin AC. Calcium channel auxiliary alpha2delta and beta subunits: trafficking and one step beyond. *Nat Rev Neurosci*. 2012;13(8):542–555. <https://doi.org/10.1038/nrn3311>.
54. Lai X, Price C, Modla S, et al. The dependences of osteocyte network on bone compartment, age, and disease. *Bone Res*. 2015;3(1):3. <https://doi.org/10.1038/boneres.2015.9>.
55. Galea GL, Price JS, Lanyon LE. Estrogen receptors' roles in the control of mechanically adaptive bone (re)modeling. *Bonekey Rep*. 2013;2:413. <https://doi.org/10.1038/bonekey.2013.147>.
56. Aguirre JI, Plotkin LI, Gortazar AR, et al. A novel ligand-independent function of the estrogen receptor is essential for osteocyte and osteoblast mechanotransduction. *J Biol Chem*. 2007;282(35):25501–25508. <https://doi.org/10.1074/jbc.M702231200>.
57. Zaman G, Jessop HL, Muzylak M, et al. Osteocytes use estrogen receptor alpha to respond to strain but their ERalpha

- content is regulated by estrogen. *J Bone Miner Res Off J Am Soc Bone Miner Res.* 2006;21(8):1297–1306. <https://doi.org/10.1359/jbmr.060504>.
58. Khosla S, Oursler MJ, Monroe DG. Estrogen and the skeleton. *Trends Endocrinol Metab.* 2012;23(11):576–581. <https://doi.org/10.1016/j.tem.2012.03.008>.
59. Saxon LK, Galea G, Meakin L, Price J, Lanyon LE. Estrogen receptors alpha and beta have different gender-dependent effects on the adaptive responses to load bearing in cancellous and cortical bone. *Endocrinology.* 2012;153(5):2254–2266. <https://doi.org/10.1210/en.2011-1977>.
60. Geoghegan IP, Hoey DA, McNamara LM. Estrogen deficiency impairs integrin alphavbeta3-mediated mechanosensation by osteocytes and alters osteoclastogenic paracrine signalling. *Sci Rep.* 2019;9(1):4654. <https://doi.org/10.1038/s41598-019-41095-3>.
61. Deepak V, Kayastha P, McNamara LM. Estrogen deficiency attenuates fluid flow-induced [Ca(2+)](i) oscillations and mechanoresponsiveness of MLO-Y4 osteocytes. *FASEB J.* 2017;31(7):3027–3039. <https://doi.org/10.1096/fj.201601280R>.
62. Xu X, Yang H, Bullock WA, et al. osteocyte estrogen receptor beta (O_t-ERbeta) regulates bone turnover and skeletal adaptive response to mechanical loading differently in male and female growing and adult mice. *J Bone Miner Res Off J Am Soc Bone Miner Res.* 2023;38(1):186–197. <https://doi.org/10.1002/jbmr.4731>.